Enforcing local equilibrium of point defects near sinks in object kinetic Monte Carlo simulations

Thomas Jourdan

Enforcing local equilibrium of point defects near sinks in object kinetic Monte Carlo simulations

T. Jourdan

Université Paris-Saclay, CEA, Service de Recherches de Métallurgie Physique, 91191, Gif-sur-Yvette, France

E-mail: thomas.jourdan@cea.fr

Abstract. A model for the emission of point defects by point defect sinks is proposed for object kinetic Monte Carlo simulations. Local equilibrium of point defects in the vicinity of sinks is ensured by construction, even if elastic interactions are taken into account for the diffusion of point defects. The emission of vacancies by dislocation segments is treated in detail and validated numerically. The model is then used to simulate the annealing of a vacancy Frank loop in a system containing surfaces. Results are in overall good agreement with analytical formulas, which are based on the approximation of instantaneous equilibration of the vacancy field during the loop evolution process. For small loops the shrinkage is so rapid that this quasi-static approximation is no more valid.

Introduction

Many physical effects in materials are driven by thermal point defect generation and diffusion. For example, annealing of point defect clusters (vacancy/interstitial dislocation loops [1, 2], cavities [3], etc.) in metallic materials often involves thermal vacancy generation. Emission rate of point defects depends on the type of point defect clusters but also on their size, leading to the well-known Ostwald ripening mechanism theorized for dislocation loops [4, 5] and cavities [6, 7]. Diffusional creep [8, 9] and climb-driven creep [10, 11] are other phenomena which finely depend on emission rates of grain boundaries or dislocations.

Object kinetic Monte Carlo (OKMC) is an efficient tool to simulate point defect diffusion and microstructure evolution at the grain scale. Contrary to atomistic kinetic Monte Carlo (AKMC), which handles all atomic sites of the system, in OKMC only defects are explicitly modeled. This framework is particularly convenient to model systems containing point defects, point defect clusters and dislocations under irradiation [12, 13], especially at low temperature where point defect emission by sinks (dislocations, surfaces, point defect clusters, etc.) can be neglected. Indeed the migration of irradiation-induced point defects in the matrix followed by their absorption by sinks is simulated faithfully, by performing the successive atomic jumps in the matrix depending on the local stress state [14, 15, 16, 17].

However, the lack of intrinsic energetic model, as those used in AKMC simulations, renders emission of point defects cumbersome to simulate. For a given point defect, emission rates must be specified independently for each sink that generates this kind of point defect by thermal activation. In the OKMC framework, the emission rate is usually governed by the binding energy of point defects to sinks [18, 19, 13]. However, there is some uncertainty as to the location where the point defect is emitted and the expression of the emission rate. Two main approaches have been proposed. The first one consists in placing the defect "close" to the sink, typically at one atomic jump length, the emission rate being proportional to the surface area of the sink absorption region. Another, simpler, possibility is to use the emission rate derived in mean field methods, and to place the defect randomly in the simulation box [20]. However, both approaches cannot guarantee in general that the concentration of point defects close to the sink, resulting from the balance between absorption and emission, is in agreement with its theoretical value given by the local equilibrium assumption [21]. This is fundamentally due to the fact that the emission term is not constructed to ensure this local equilibrium of point defects. Recently, an emission model was proposed for dislocations [22], based on the seminal work of Friedel [23]. It takes into account the local stress, so it is more general than the approximation of binding energy, which is usually assumed to be an intrinsic property of the sink. Unfortunately, the ability of this model to enforce a correct local equilibrium concentration of point defects has not been numerically demonstrated.

In this article a simple yet accurate method is proposed to define emission rates in OKMC, which ensures local equilibrium around sinks. It is the case even if diffusion

is biased by local and applied stresses. The method can be applied to any kind of sink (surface, grain boundary, dislocation, cavity, etc.). In Section 1 the method is exemplified with the case of a dislocation segment. In section 2 an example involving a dislocation loop and a surface is shown and the potentialities of the method are discussed.

1. Emission model for OKMC simulations

In this section the emission model is derived for the emission of vacancies by a dislocation segment. The OKMC method used here is first briefly reminded. The local equilibrium concentration near a dislocation is then recalled. In the third subsection it is shown how to impose this concentration in an OKMC framework. Finally the numerical implementation and validation of the emission model are presented.

1.1. OKMC simulations

OKMC is a useful method to simulate the time evolution of a system containing point defects and sinks [18, 24]. The simulation box size can be as large as a few hundreds of nm, which makes it possible to consider realistic microstructures with surfaces, grain boundaries, etc. As any KMC method, OKMC uses a database of known transition rates at a given time t to determine the next state of the system and the required increment of time Δt to perform the chosen transition, following the residence time algorithm [25, 26]. In the present simulations, transitions are of two kinds: the jump of a vacancy from one stable position to another one and the thermal creation of a vacancy by a sink. The determination of transitions corresponding to the thermal generation of a defect is the objective of this work.

Transitions corresponding to atomic jumps are simple to consider. The new state of the system is obtained by moving the chosen point defect from its current position $\boldsymbol{r}$ by the jump vector $\boldsymbol{h}_j$ corresponding to the selected jump j ($j = 1, \ldots, z$ where z is the total number of jumps for a point defect). The associated jump frequency is

$$\omega_{\cdot\to j}(\boldsymbol{r}) = \nu_0 \exp\left(-\frac{\Delta E_{\cdot\to j}(\boldsymbol{r})}{k_\mathrm{B}T}\right), \tag{1}$$

where ν_0 is an attempt frequency and $\Delta E_{\cdot\to j}$ is the activation energy, given by

$$\Delta E_{\cdot\to j}(\boldsymbol{r}) = E^\mathrm{m} + E^{\mathrm{int,sad}}_{\cdot\leftrightarrow j}(\boldsymbol{r} + \boldsymbol{h}_j/2) - E^{\mathrm{int,sta}}(\boldsymbol{r}). \tag{2}$$

In this equation E^m is the migration energy in the bulk, without any effect of stress, $E^{\mathrm{int,sta}}(\boldsymbol{r})$ and $E^{\mathrm{int,sad}}_{\cdot\leftrightarrow j}(\boldsymbol{r} + \boldsymbol{h}_j/2)$ are the interaction energies of the defect with the local elastic field at its initial stable position and at the saddle position, respectively. Although the saddle is not required to be located halfway between the two stable positions, this notation is used for clarity. The subscript "$\cdot \leftrightarrow j$" is to mention that the interaction energy at saddle position from $\boldsymbol{r}$ to $\boldsymbol{r} + \boldsymbol{h}_j$ is assumed to be the same as the interaction

energy from $\boldsymbol{r} + \boldsymbol{h}_j$ to $\boldsymbol{r}$. Point defects like vacancies or self-interstitial atoms (SIAs) are conveniently described by their double force tensor $\boldsymbol{P}$ [27], so the interaction energy reads

$$E^{\mathrm{int,sta}}(\boldsymbol{r}) = -P^{\mathrm{sta}}_{kl}\varepsilon_{kl}(\boldsymbol{r}) \tag{3}$$

$$E^{\mathrm{int,sad}}_{\cdot\leftrightarrow j}(\boldsymbol{r}) = -P^{\mathrm{sad},j}_{kl}\varepsilon_{kl}(\boldsymbol{r}), \tag{4}$$

where $\boldsymbol{\varepsilon}(\boldsymbol{r})$ is the strain tensor at the location of the point defect (summation over repeated indices is implied). Since vacancies are isotropic at their stable position in body centered and face centered cubic lattices, there is only one variant of this defect at stable position and therefore a single value of $\boldsymbol{P}^{\mathrm{sta}}$. It is not the case for the saddle configuration, that is why $\boldsymbol{P}^{\mathrm{sad}}$ depends on the jump considered. For SIAs, it is necessary to use the dipole tensor corresponding to the stable configuration considered.

In the following OKMC is used in an "off-lattice" mode: although point defects perform atomic jumps in the directions given by the lattice orientation, they are not necessarily created at true lattice positions. This approach is more handy when disruptions of the perfect lattice are present due to, for example, dislocations. Using the true lattice positions would require storing them, which would increase the memory footprint and complexity of the code. The off-lattice OKMC mode can be viewed as a way to simulate the evolution of defects based on continuous diffusion models [28]. Local defect concentrations can be extracted from OKMC simulations by recording the time spent by all defects in a small volume and dividing it by the total time of recording and by the volume. However, there are no concentration variables in OKMC, contrary to continuous models, so OKMC simulations do not require to mesh the system to determine its time evolution. The memory footprint in OKMC simulations is therefore often much lower.

1.2. Local equilibrium concentration near a dislocation

Local equilibrium around a sink results from the fact that the sink can both absorb and emit point defects efficiently. The local equilibrium concentration around a dislocation can be obtained by requiring that there is no change in the free energy of the solid when a point defect is emitted by the dislocation. The sum of the work of the osmotic and Peach-Köhler forces must therefore be zero [29]. In the case of vacancies, for a dislocation of Burgers vector $\boldsymbol{b}$ and sense $\boldsymbol{\xi}$, it leads to

$$C_v^{\mathrm{eq,loc}}(\boldsymbol{r}) = C_v^{\mathrm{eq}} \exp\left(-\frac{E^{\mathrm{int,sta}}(\boldsymbol{r})}{k_{\mathrm{B}}T}\right) \exp\left(\frac{[(\boldsymbol{b}\cdot\boldsymbol{\sigma})\times\boldsymbol{\xi}]\cdot(\boldsymbol{b}\times\boldsymbol{\xi})}{|\boldsymbol{b}\times\boldsymbol{\xi}|^2}\frac{\Omega}{k_{\mathrm{B}}T}\right). \tag{5}$$

In this equation C_v^{eq} is the equilibrium concentration of vacancies in absence of internal and applied stresses, $\boldsymbol{\sigma}$ is the stress field on the dislocation and Ω is the atomic volume. The equilibrium concentration can be written

$$C_v^{\mathrm{eq}} = \frac{1}{\Omega}\exp\left(-\frac{E_v^{\mathrm{f}}}{k_{\mathrm{B}}T}\right), \tag{6}$$

where E_v^{f} is the formation energy of a vacancy. In body centered and face centered cubic lattices the dipole tensor of a vacancy in its stable configuration is simply $P_{ij} = K\Delta V_v^{\mathrm{r}}\delta_{ij}$, with K the bulk modulus, ΔV_v^{r} the relaxation volume and δ_{ij} the Kronecker delta. The interaction energy becomes

$$E^{\mathrm{int,sta}}(\boldsymbol{r}) = (p^{\mathrm{a}} + p^{\mathrm{i}}(\boldsymbol{r}))\Delta V^{\mathrm{r}}, \tag{7}$$

where $p^{\mathrm{X}} = -\sigma_{ii}/3$ is the pressure and label X refers either to the applied stress (X = a) or internal stress (X = i). For an isolated dislocation, sufficiently far from it p^{i} is negligible. If in addition, the external applied stress corresponds to a pure hydrostatic pressure, Equation (5) takes the well known form [29]

$$C_v^{\mathrm{eq,loc}} = C_v^{\mathrm{eq}} \exp\left(-\frac{p^{\mathrm{a}}(\Delta V_v^{\mathrm{r}} + \Omega)}{k_{\mathrm{B}}T}\right). \tag{8}$$

1.3. Imposing the equilibrium concentration in OKMC near a dislocation

In this section we want to determine an emission rate of defects which ensures that local equilibrium concentration is obtained close to the sink. We consider the case of vacancies, which only have a single variant at stable position. The following approach is easily generalized to a defect with several variants, such as SIAs. Let us consider a small volume δV around a position $\boldsymbol{r}$ close to a dislocation. It is assumed to be small enough so that the concentration is approximately constant over δV. The local concentration in δV, noted $C_v(\boldsymbol{r})$ can be extracted from OKMC. Its equivalent evolution equation reads:

$$\frac{\mathrm{d}C_v(\boldsymbol{r})}{\mathrm{d}t} = G_v(\boldsymbol{r}) - \sum_{j=1}^{z} \omega_{\cdot\to j}(\boldsymbol{r})C_v(\boldsymbol{r}) + \sum_{j=1}^{z} \omega_{j\to\cdot}(\boldsymbol{r})C_v(\boldsymbol{r}+\boldsymbol{h}_j)\eta_j. \tag{9}$$

Similarly to Eq. (1), $\omega_{j\to\cdot}(\boldsymbol{r})$ is the jump frequency from neighbour site j, located at $\boldsymbol{r}+\boldsymbol{h}_j$:

$$\omega_{j\to\cdot}(\boldsymbol{r}) = \nu_0 \exp\left(-\frac{\Delta E_{j\to\cdot}(\boldsymbol{r})}{k_{\mathrm{B}}T}\right), \tag{10}$$

with

$$\Delta E_{j\to\cdot}(\boldsymbol{r}) = E_v^{\mathrm{m}} + E_{\cdot\leftrightarrow j}^{\mathrm{int,sad}}(\boldsymbol{r}+\boldsymbol{h}_j/2) - E^{\mathrm{int,sta}}(\boldsymbol{r}+\boldsymbol{h}_j). \tag{11}$$

The factor η_j takes two different values : $\eta_j = 1$ if $\boldsymbol{r}+\boldsymbol{h}_j$ is in the matrix and $\eta_j = 0$ if $\boldsymbol{r}+\boldsymbol{h}_j$ is in the capture region of the dislocation. G_v is a creation rate to impose local equilibrium concentration. This creation rate remains to be determined.

At equilibrium, Equation (9) becomes:

$$G_v(\boldsymbol{r}) - \sum_{j=1}^{z} \omega_{\cdot\to j}(\boldsymbol{r})C_v^{\mathrm{eq,loc}}(\boldsymbol{r}) + \sum_{j=1}^{z} \omega_{j\to\cdot}(\boldsymbol{r})C_v^{\mathrm{eq,loc}}(\boldsymbol{r}+\boldsymbol{h}_j)\eta_j = 0. \tag{12}$$

Since $C_v^{\mathrm{eq,loc}}$ is known owing to Eq. (5), the creation rate necessary to impose local equilibrium concentration is determined by Eq. (12). This expression can be simplified

if it is assumed that the factor related to the Peach-Köhler force is the same for $\boldsymbol{r}$ and all positions $\boldsymbol{r}+\boldsymbol{h}_j$. This is usually a good approximation, which cannot be made for $E^{\mathrm{int,sta}}(\boldsymbol{r})$ due to the sharp variation of $\varepsilon_{ij}(\boldsymbol{r})$ close to the dislocation. Equation (12) becomes

$$G_v(\boldsymbol{r}) = \left[\sum_{j=1}^{z} \omega_{\cdot\to j}(\boldsymbol{r}) C_v^{\mathrm{eq}} \exp\left(-\frac{E^{\mathrm{int,sta}}(\boldsymbol{r})}{k_{\mathrm{B}}T}\right) - \sum_{j=1}^{z} \omega_{j\to\cdot}(\boldsymbol{r}) C_v^{\mathrm{eq}} \exp\left(-\frac{E^{\mathrm{int,sta}}(\boldsymbol{r}+\boldsymbol{h}_j)}{k_{\mathrm{B}}T}\right)\eta_j\right] \times \exp\left(\frac{[(\boldsymbol{b}\cdot\boldsymbol{\sigma})\times\boldsymbol{\xi}]\cdot(\boldsymbol{b}\times\boldsymbol{\xi})}{|\boldsymbol{b}\times\boldsymbol{\xi}|^2}\frac{\Omega}{k_{\mathrm{B}}T}\right). \quad (13)$$

Inserting Eqs. (1)-(2) and (10)-(11) in Eq. (13) leads to

$$G_v(\boldsymbol{r}) = \nu_0 C_v^{\mathrm{eq}} \exp\left(-\frac{E_v^{\mathrm{m}}}{k_{\mathrm{B}}T}\right)\left[\sum_{j=1}^{z} \exp\left(-\frac{E_{\cdot\leftrightarrow j}^{\mathrm{int,sad}}(\boldsymbol{r}+\boldsymbol{h}_j/2)}{k_{\mathrm{B}}T}\right)(1-\eta_j)\right] \times \exp\left(\frac{[(\boldsymbol{b}\cdot\boldsymbol{\sigma})\times\boldsymbol{\xi}]\cdot(\boldsymbol{b}\times\boldsymbol{\xi})}{|\boldsymbol{b}\times\boldsymbol{\xi}|^2}\frac{\Omega}{k_{\mathrm{B}}T}\right) \quad (14)$$

This equation deserves some comments:

- The emission rate at a given location is zero if there is no jump from this location to the capture region of the dislocation ($\eta_j = 1$ for all neighbours). The emission is therefore limited to a region around the dislocation. For a dislocation whose capture region is a cylinder of radius r_{c}, the emission region is bounded by a cylinder of radius $r_{\mathrm{e}} = r_{\mathrm{c}} + d_{\max}$, where $d_{\max}$ is the maximum jump distance.
- The number of jumps which connect the point defect to the capture region varies as the point defect approaches the dislocation core. The variation of $(1-\eta_j)$ from 0 to 1 leads to sharp spatial variations of the emission rate. Therefore it is necessary to evaluate the emission rate at several locations to obtain a good balance between emission and absorption (statistically, with off-lattice OKMC all locations outside the capture region are explored by point defects). In practice, it is done by meshing the emission region and evaluating the emission rates on the mesh.
- The emission rate does not depend on the interaction energy *at stable point*. In other words, for an isotropic defect at stable point, such as a vacancy, the emission rate is independent of its relaxation volume. It depends on the interaction energy *at saddle point* of the jumps from the emission location to the capture region of the dislocation. This is at variance with the approach derived by McElfresh *et al.* [22], which depends only on the interaction energy at stable point, through $C_v^{\mathrm{eq,loc}}$.
- The emission rate does not depend on the supersaturation level, as it should be [23].

1.4. Numerical implementation of the emission model

As mentioned in the previous section, the emission model requires meshing the emission region around the sink. For a straight dislocation, it has the natural cylindrical

symmetry (Fig. 1). The emission rate inside an elementary emission volume is given by

$$P_i = G_v(\boldsymbol{r}_i)V_i, \tag{15}$$

where i refers to the considered volume and $V_i = 1/2(r_1 + r_2)(r_2 - r_1)\Delta\theta\Delta l = 1/2(r_1 + r_2)\Delta r\Delta\theta\Delta l$. The position $\boldsymbol{r}_i$ is chosen in the middle of the emission volume.

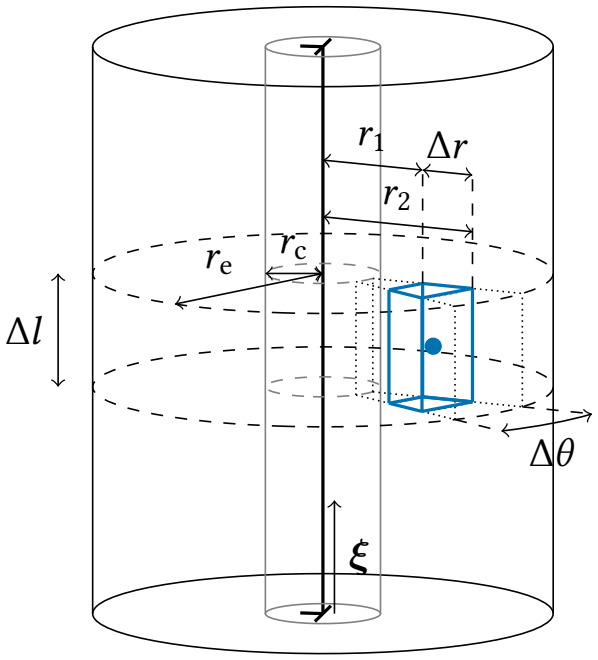

Figure 1. Schematics of the emission region around an edge dislocation segment. An elementary emission volume is shown in blue, the emission point is given by the blue dot.

In the present approach, emission occurs everywhere along the dislocation segment. In fact, point defects can be emitted only at jogs, so the model corresponds to a dislocation saturated with jogs. This approximation is more satisfactory at high temperature, high supersaturation or subsaturation of point defects [30, 31] or, for example, if the dislocation segment is located in some parts of a rounded dislocation loop which are known to be heavily jogged [1]. It may also represent a more general situation with lower jog density but fast pipe diffusion. In this case the climb of dislocations is limited by the diffusion of point defects in the bulk and dislocations maintain local equilibrium concentration of defects all along their line [32].

The values of Δl, $\Delta\theta$, and Δr should be sufficiently small to ensure a correct local equilibrium concentration around the dislocation segment. Although the discretization could in principle be chosen arbitrarily small, increasing the number of emission volumes may impair the numerical efficiency of the code. It is thus interesting to identify optimal values of the parameters on a test case.

For this purpose we consider a dislocation dipole, as shown in Fig. 2-(a). Parameters are typical of aluminum (Tab. 1) and the strain field generated by the dipole is calculated

Table 1. Material parameters for Al used in this study.

Parameter	Symbol	Value	Reference
Lattice parameter	a_0	0.405 nm	
Atomic volume	Ω	$a_0^3/4 = 0.0167$ nm^3	
Poisson's ratio	ν	0.35	[17]
Shear modulus	μ	26 GPa	[17]
Maximum jump distance	$d_{\max}$	$a_0/\sqrt{2} = 0.286$ nm	
Capture radius of dislocations	r_c	0.57 nm	
Core width (for strain field calculation)	a	0.05 nm	
Burgers vector	$\boldsymbol{b}$	1/3[111]	
Formation energy	E_v^f	0.67 eV	[33]
Migration energy	E_v^m	0.605 eV	[17]
Attempt frequency	ν_0	10^{13} Hz	
Elastic dipole for vacancies at stable position	$\boldsymbol{P}_v^{sta}$	$\begin{bmatrix} -3.238 & 0 & 0 \\ 0 & -3.238 & 0 \\ 0 & 0 & -3.238 \end{bmatrix}$ eV	[17]
Elastic dipole for vacancies at saddle position (jump in [110] direction)	$\boldsymbol{P}_v^{sad}$	$\begin{bmatrix} -2.866 & -0.080 & 0 \\ -0.080 & -2.866 & 0 \\ 0 & 0 & 1.000 \end{bmatrix}$ eV	[17]
Intrinsic stacking fault energy	γ	0.166 J m^{-2}	[29]

using isotropic elasticity. The Burgers vector is $\pm 1/3[111]$, corresponding to a Frank partial dislocation. This choice is motivated by the study of the next section, which focuses on the evolution of vacancy Frank loops. Several orientations of crystallographic axes are considered by rotating the lattice around the [111] direction by an angle α. This allows us to investigate whether all segments of a Frank dislocation loop are properly handled by the method.

Emission rates are shown in Fig. 2-(b,c) for two values of α ($\alpha = 0$ and $\alpha = 90°$). They vary significantly from one emission volume to another one. This variation is explained by two different factors. The first one is the different number of atomic jumps from the center of emission volumes into the capture region of the dislocation segment. Only these jumps contribute to the emission rate (Eq. (14)). This explains why, for example, emission rates are higher close to the dislocation. The second factor is the value of the interaction energy at saddle position. Since the strain field varies sharply around the dislocation and the values of dipole tensors at saddle position depend on the jump direction, the emission rate is also highly dependent on the emission volume considered.

These two factors also explain the difference of emission rates when α is varied. We note that when α changes, the jump directions change and the values of interaction energies are also modified. Even if the energy is calculated at the same location for two values of α, the interaction energy is not the same since the dipole tensor at saddle point, which is not isotropic, must be rotated according to the rotation of the crystallographic

axes.

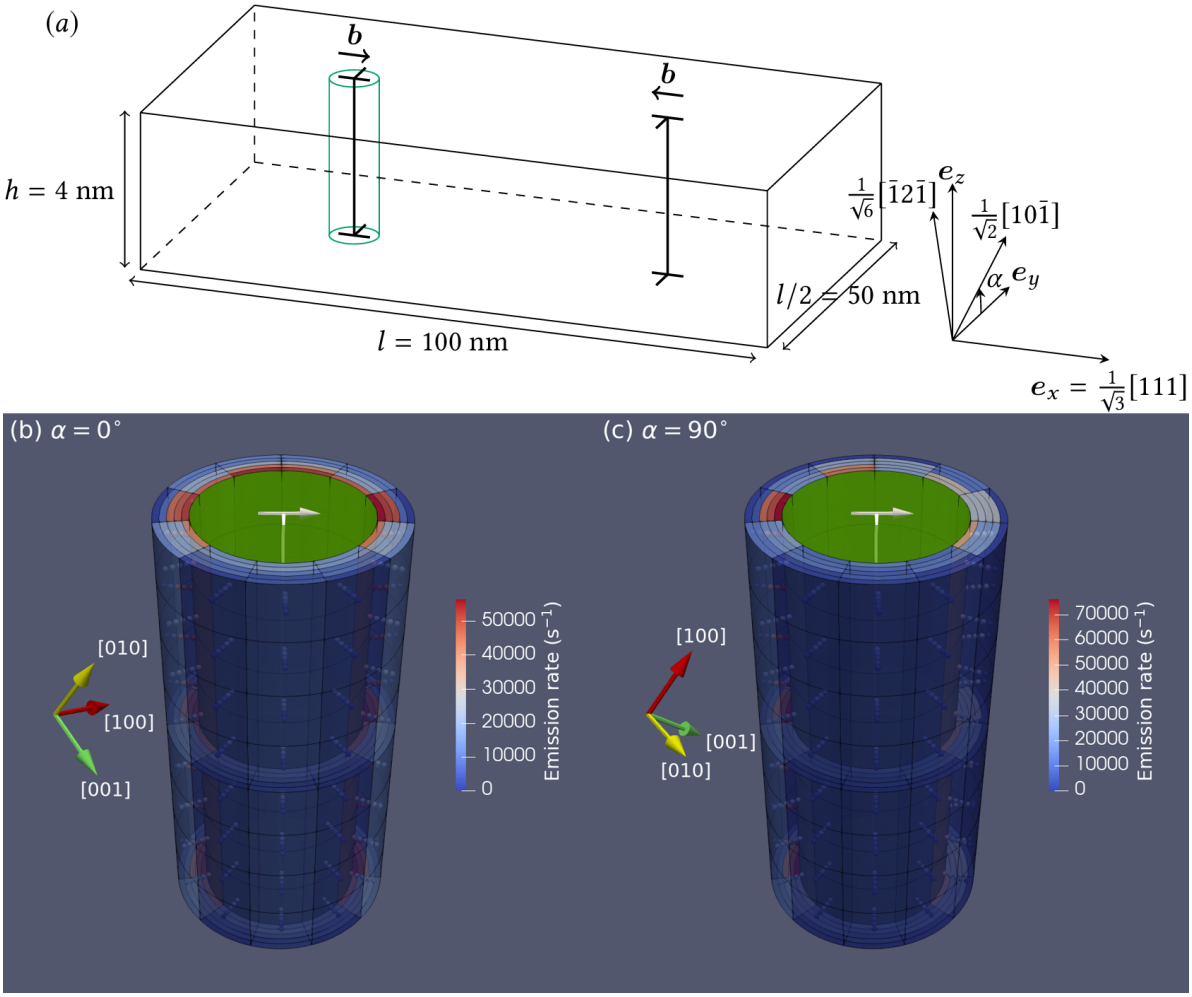

Figure 2. Schematics of the dislocation configuration used to determine optimal discretization parameters and examples of emission rates. (a) Simulation box containing the two Frank partial dislocations. The angle α can be varied to rotate the crystallographic axes, while keeping the same dislocation configuration in the box. (b,c) Emission rates of dislocation segments for two values of α ($\alpha = 0$ and $\alpha = 90°$), for the dislocation identified by a green cylinder in (a). Each dislocation contains two segments of 2 nm and the discretization parameters are $\Delta l = 0.5$ nm, $\Delta\theta = 16.4°$ and $\Delta r = 0.06$ nm. Points where emission rates are calculated are shown by a sphere in each emission volume.

To evaluate the local equilibrium concentration, the following simulation setup is used. Initially the OKMC box contains only the two dislocations and the temperature is set to 700 K. Vacancies start to be emitted by the dislocations so their number increases in the box, until it reaches a stationary value. From this time the vacancy concentration is recorded and averaged. An estimate of the standard error of the mean is obtained by a block average technique [34]. Since the two straight dislocations are the only sinks in the box and no external stress is applied, the average concentration in the box should correspond to the equilibrium concentration (Eqs. (6) and (8), with $p^{\mathrm{a}} = 0$).

Results are shown in Fig. 3 for three different discretizations. Even with a very fine discretization along the tangential direction (21 points, $\Delta\theta = 8.6^\circ$), results are not very accurate if only a single emission volume is used along the radial direction ($\Delta r = 0.29$ nm). Using five discretization points ($\Delta r = 0.06$ nm) improves significantly the agreement with Eq. (6), even with as low as 11 discretization points along the tangential direction ($\Delta\theta = 16.4^\circ$). Adding more points along the radial direction ($\Delta r = 0.02$ nm) proves useless in the present case. In the following we will use the parameters $\Delta\theta = 16.4^\circ$ and $\Delta r = 0.06$ nm. Concerning the discretization length along the dislocation line Δl, a generic value cannot be given, since it depends on the local curvature of the dislocation. However, a value of the order of a few angstroms has proved to be small enough for the cases studied. Here, $\Delta l = 0.5$ nm has been adopted. In this specific calculation, the number of emission volumes has a negligible influence on the computation time. This is because the sink does not evolve and emission rates are calculated only once at the beginning of the simulation. However, in the general case of evolving sinks, emission rates must be recalculated every time a point defect is emitted or absorbed. The computation time of this step varies linearly with the number of emission volumes.

The emission model described in this work can be easily applied to other types of sinks: grain boundaries, surfaces, cavities, etc. In each case, a small emission region of width $d_{\max}$ must be defined around the sink. Emission rates are given by expressions similar to Eq. (14). For instance, the Gibbs-Thomson effect must be included in the emission rate of a cavity. Apart from the discretization, which must be adapted to each geometry, the method remains essentially the same. Although emission of point defects has been assumed to occur over the whole surface of the sink, more complex situations could be envisaged. For example, as a first approximation jogs in dislocation lines may be introduced in the formalism by enabling absorption and emission of point defects only at particular locations [30, 31].

2. Application of the emission model: Annealing of dislocation loops in finite systems

Annealing of dislocation loops has been studied experimentally [1, 35, 36, 37, 2] and numerically [38, 39, 40, 41]. The driving force for the loops' evolution is their line tension and their surface tension if they are faulted. Here we consider the annealing of a single vacancy Frank loop in a system containing free surfaces in the three directions. This condition may represent, as least in a qualitative manner, the annealing of a loop in a thin foil geometry more often observed experimentally. The choice of the free surfaces in the three directions instead of only one is made to be more representative of the geometries used to derive analytical expressions. For a dislocation loop of radius r with a surface at infinity, the shrinking rate has been obtained by solving the diffusion equation around the toroidal sink [42, 43]. The following assumptions are made:

- The effect of stress field on diffusion is neglected.

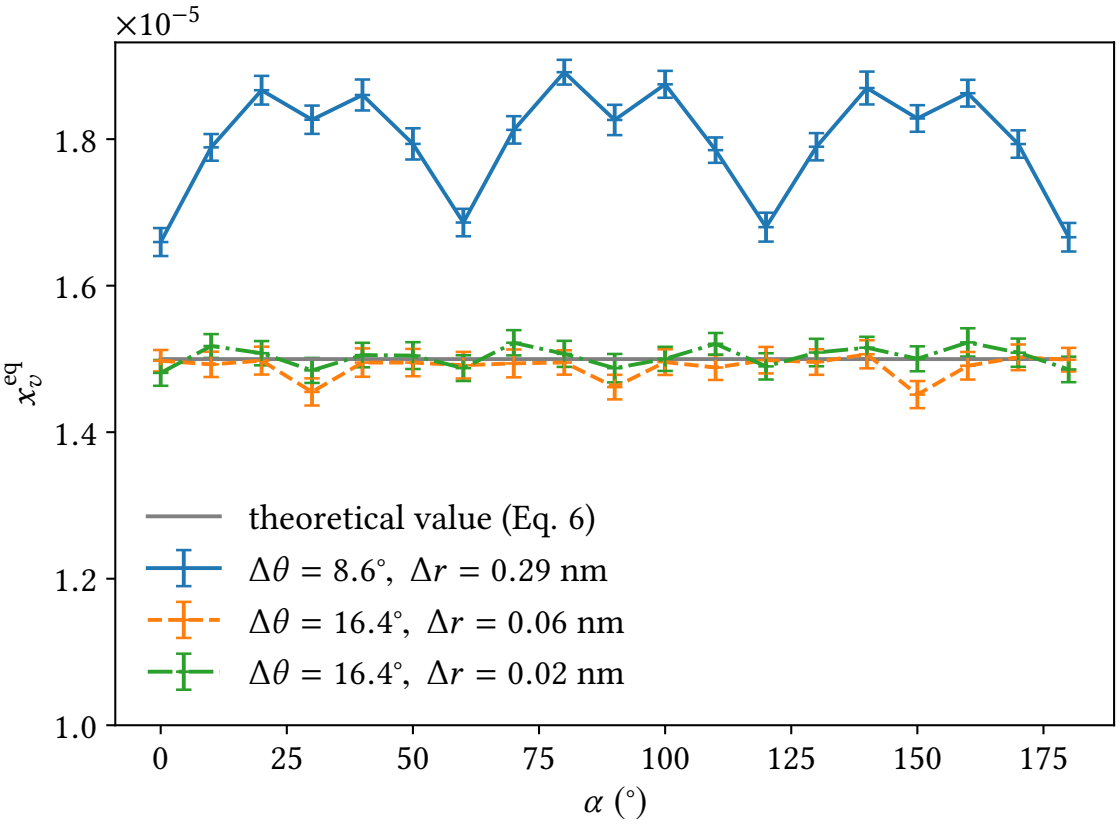

Figure 3. Atomic fraction of vacancies in a box containing two straight dislocations, as a function of angle α (see Fig. 2). Values $\Delta\theta = 8.6°$ and 16.4° correspond to a number of emission volumes equal to 21 and 11 respectively. The number of emission volumes in the radial direction is 1, 5 and 11 for values of Δr equal to 0.29, 0.06 and 0.02 nm respectively.

- The diffusion of vacancies is sufficiently fast to ensure equilibrium with the surface at each time, so the steady-state concentration profile can be used to estimate the vacancy flux to or from the loop.
- The kinetics is diffusion-limited, so the dislocation loop and surfaces maintain local equilibrium of point defects in their vicinity.

If in addition $r \gg r_{\mathrm{c}}$, the shrinking rate is approximately given by

$$\frac{\mathrm{d}r}{\mathrm{d}t} = \frac{2\pi}{\ln\left(\frac{8r}{r_{\mathrm{c}}}\right)} \frac{\Omega}{b} D_v \left(C_v^{\mathrm{eq}} - C_v^{\mathrm{eq}} \exp\left(-\frac{f_{\mathrm{cl}}(r)\Omega}{b k_{\mathrm{B}} T} \right) \right), \tag{16}$$

with f_{cl} the climb force which reads

$$f_{\mathrm{cl}}(r) = -\frac{\mu b^2}{4\pi(1-\nu)r} \ln\left(\frac{8r}{a}\right) - \gamma. \tag{17}$$

The first term in the parenthesis of Eq. (16) is due to the surfaces at infinity, which impose $C_v = C_v^{\mathrm{eq}}$. The second term corresponds to the local equilibrium concentration

close to the loop. In Eq. (17), γ is the intrinsic stacking fault energy and a is the core width defined in the non-singular theory of dislocations of Cai *et al.* [44]. The diffusion coefficient of the vacancy is $D_v = \nu a_0^2 \exp\left(-E_v^{\mathrm{m}}/k_{\mathrm{B}}T\right)$.

Equations similar to (16) have been used successfully to reproduce experimental results of annealing of loops in aluminum [35]. In particular, it was shown that a model based on the emission of vacancies at jogs could only reproduce a part of the experimental results, whereas a model based on diffusion-limited kinetics as in Eq. (16) could account for the complete annealing process. This indicates that dislocation loops in aluminum are efficient sinks [32, 30] and validates the assumption of local equilibrium concentration of point defects all along their core. Recent calculations on straight dislocations in aluminum tend to confirm this conclusion [31, 45].

Some previous works [46, 47] suggest that this expression can be generalized for a finite system with an outer spherical boundary of radius R_{ext} where C_v^{eq} is imposed, leading to

$$\frac{\mathrm{d}r}{\mathrm{d}t} = \frac{2\pi}{\ln\left(\frac{8r}{r_{\mathrm{c}}}\right)} \frac{1}{1 - \frac{2\pi}{\ln\left(\frac{8r}{r_{\mathrm{c}}}\right)} \frac{r}{2R_{\mathrm{ext}}}} \frac{\Omega}{b} D_v \left(C_v^{\mathrm{eq}} - C_v^{\mathrm{eq}} \exp\left(-\frac{f_{\mathrm{cl}}(r)\Omega}{b k_{\mathrm{B}} T} \right) \right). \tag{18}$$

In the following the loop is described as a torus in the OKMC code, in agreement with the analytical approach. This description is adopted for the generation of the strain field and for the emission model, leading to a toroidal meshing. The loop could also have been described as a collection of straight dislocation segments, but this discretization in straight lines could introduce spurious effects on results, making this approach less faithful to the analytical one. The temperature is set to 500 K for all simulations.

As in the previous section, the toroidal discretization is first validated by comparing the concentration in a box containing a loop but no surface to the theoretical one (second term of Eq. (16)). Periodic boundary conditions are used in a box of size $50\times50\times50$ nm^3. The loop can emit vacancies but its size is kept constant. As shown in Fig. 4, with the parameters used in the previous section, the agreement with the theoretical value is very good, even for loops as small as 1.5 nm.

We now consider a system with free surfaces in the three directions of space. The emission model presented in this work for dislocation segments has been adapted to surfaces, by meshing a slice close to each surface. The strain field generated by the loop in the finite system is taken the same as in the infinite medium. For the smallest system (50 nm) and the largest loop (radius of 5 nm), the maximal surface tractions created by the loop are about 28 MPa. A rough estimate of the modification of migration barriers due to this stress is $\sigma\Delta V_v^{\mathrm{r}} \approx 1$ meV. Such energy changes are too small to have an appreciable influence on the point defect kinetics. This is in line with a previous study, where stresses of several hundreds of MPa have been shown to be necessary to modify the defect kinetics in Al at 300 K [48]. Since stress effects on diffusion decrease as temperature increases, this validates the approximation of infinite medium for the elastic solution in the present conditions.

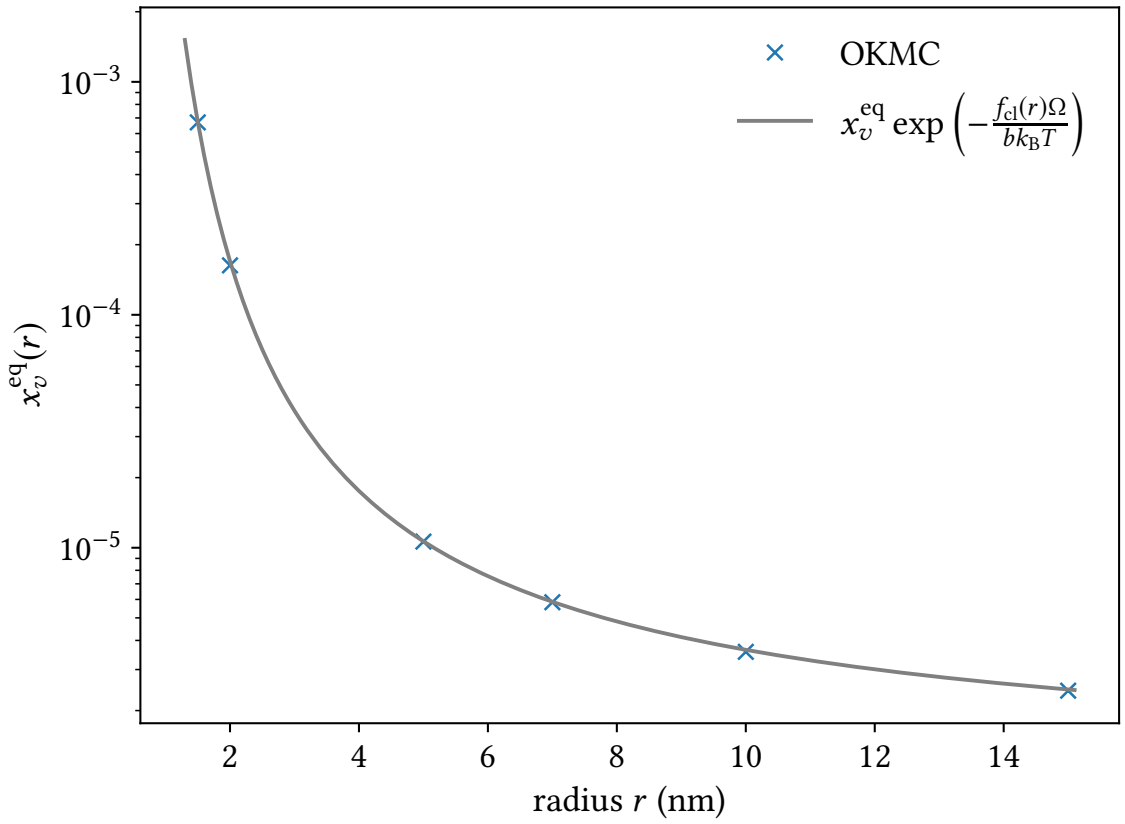

Figure 4. Local equilibrium atomic fraction of vacancies close to a vacancy Frank loop at 500 K. The OKMC value is obtained by averaging the number of vacancies in a box of size $50 \times 50 \times 50$ nm^3 containing a single dislocation loop.

The system is first equilibrated with a constant-size loop. Once vacancy concentration has reached its steady state value, the loop radius is no more constrained and the vacancy loop starts shrinking due to its line and surface tensions. This is the starting point of the simulations shown in Fig. 5, for three system sizes (50, 100 and 200 nm). Each result is the average of 100 independent simulations, except close to the final time if some loops have already disappeared. A simulation is stopped when the loop is too small for a toroidal discretization to be used. Here it occurs as soon as $r \leq 1.2$ nm. In this case it is assumed that the loop disappears so quickly that it can be included as a zero size loop in the calculation of the average radius for the next output time steps. This is why on average, the radius can be lower than 1.2 nm. However, it should be kept in mind that this approximation leads to a slight underestimation of the average radius.

The overall agreement between OKMC and the analytical result for an infinite system (Eq. (16)) is correct for small times, for $l = 100$ and 200 nm. However, if the system's size is smaller ($l = 50$ nm), the initial slope is clearly different. In all cases, the OKMC results depart from the analytical solution when the loop becomes small. This

discrepancy is more obvious for small systems. Using the approximate solution for a finite system (Eq. (18)) improves significantly the agreement with OKMC. The difference between OKMC and the analytical solution becomes independent of the system's size, which validates Eq. (18) as a generalization of Eq. (16) for finite systems.

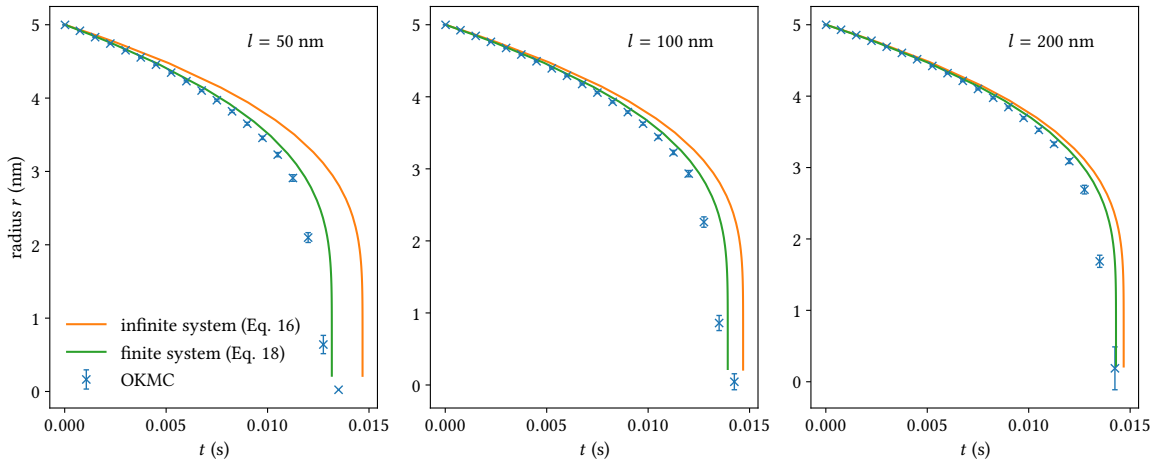

Figure 5. Evolution of a loop in a cubic system of edge's length 50, 100 and 200 nm, with free surfaces. OKMC results are obtained by averaging loop sizes over 100 simulations, except for the last iterations where some loops already disappeared. Solutions for an infinite and a finite system correspond to the integration of Eqs. (16) and (18) respectively.

Eqs. (16) and (18) assume that the vacancy concentration field remains at equilibrium at each time. Recently it has been shown that for vacancy loops in tungsten, the time for vacancy equilibration is shorter than the characteristic time for loop evolution [41], which validates this hypothesis. This means that vacancies have time to diffuse in the system, before the equilibrium vacancy concentration profile changes appreciably due to a change in the microstructure. This quasi-static approximation has been shown to be more justified for large loops, which induce smaller concentration changes as they evolve.

The model presented here does not assume that the microstructure is quasi-static. Therefore it can be used to check if this approximation is always valid. As can be seen in Fig. 6-(a,b), while the analytical formula for a finite system reproduces accurately the OKMC result for a loop of radius 5 nm, it fails for a loop of radius 2 nm. This may point to an effect of the concentration field transient. A first answer is given by the average concentration in the system, which is recorded during the loop evolution. As discussed previously, the toroidal discretization requires a loop radius larger than 1.2 nm, otherwise the simulation is stopped. For subsequent output time steps, the simulation does not contribute anymore to the average vacancy concentration but it contributes as zero to the average radius, so there is no more rigorous link between the average radius and the average concentration. To avoid any misinterpretation, the concentration is not displayed as soon as some simulations have stopped (Fig. 6-(c,d)). In addition to

the instantaneous vacancy concentration, an equilibrium vacancy concentration can be obtained at each output time step by running OKMC simulations with the loop size kept constant and taken as the average size at this time step.

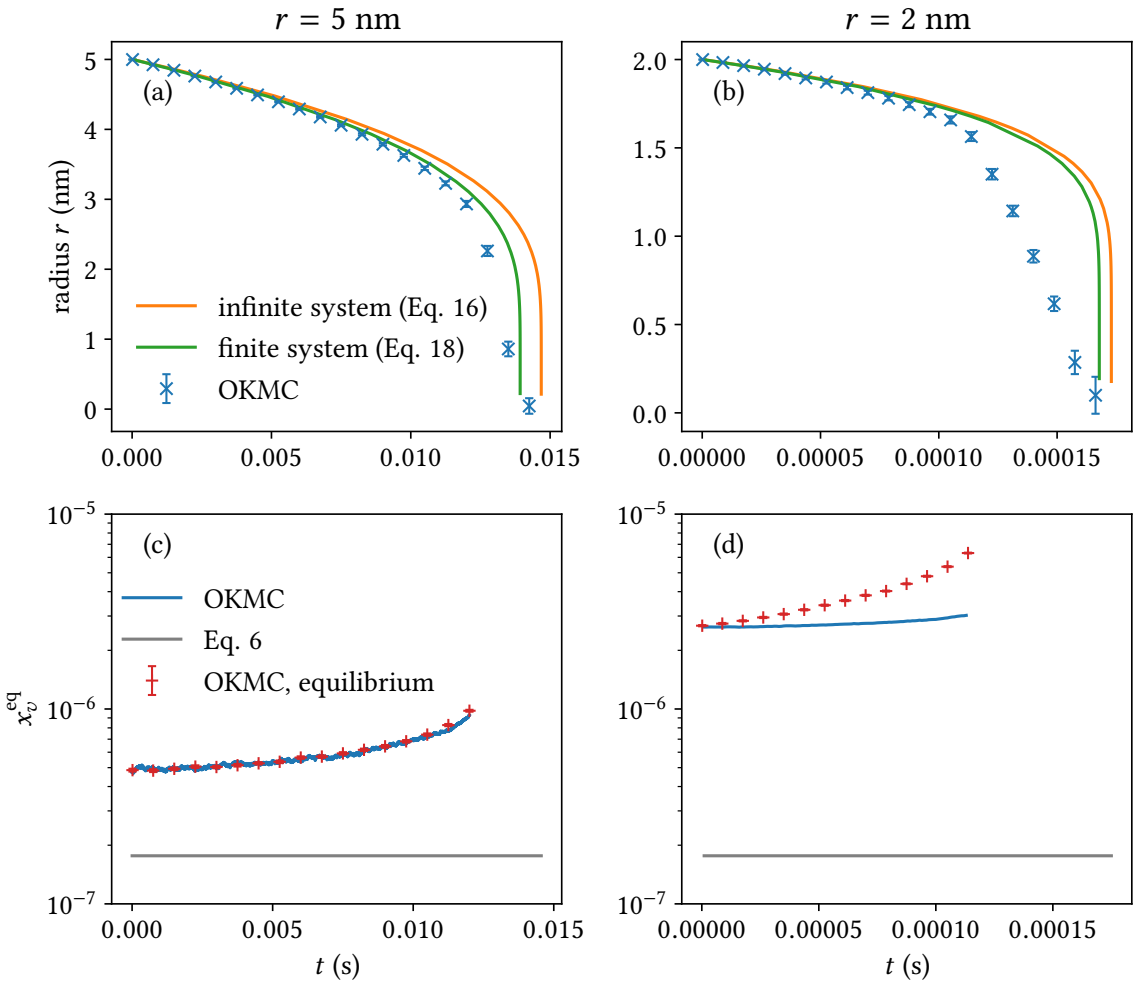

Figure 6. Evolution of a cubic system of size 100 nm containing a vacancy Frank loop of initial radius 2 or 5 nm. (a,b) Loop radius given by OKMC and by analytical solutions (Eqs. (16) and (18)). (c,d) Vacancy atomic fraction. The equilibrium value in OKMC is obtained at each timestep by setting the loop size to its value given in Figs. (a) and (b) and running the code with fixed loop radius.

The instantaneous and equilibrium values are shown in Fig. 6-(c,d). They are close to each other for $r = 5$ nm, whereas for $r = 2$ nm the equilibrium value is systematically above the instantaneous value. The source of this discrepancy is visible in Fig. 7, where the instantaneous vacancy concentration profiles are compared to the equilibrium concentration profiles at the same time and to the initial equilibrium profiles. For a loop of size $r = 5$ nm, the instantaneous profile coincides with the equilibrium profile. Close to the loop of size $r = 2$ nm, the concentration profile is the same as the equilibrium one, while far from the loop it is superimposed on the initial equilibrium profile. This

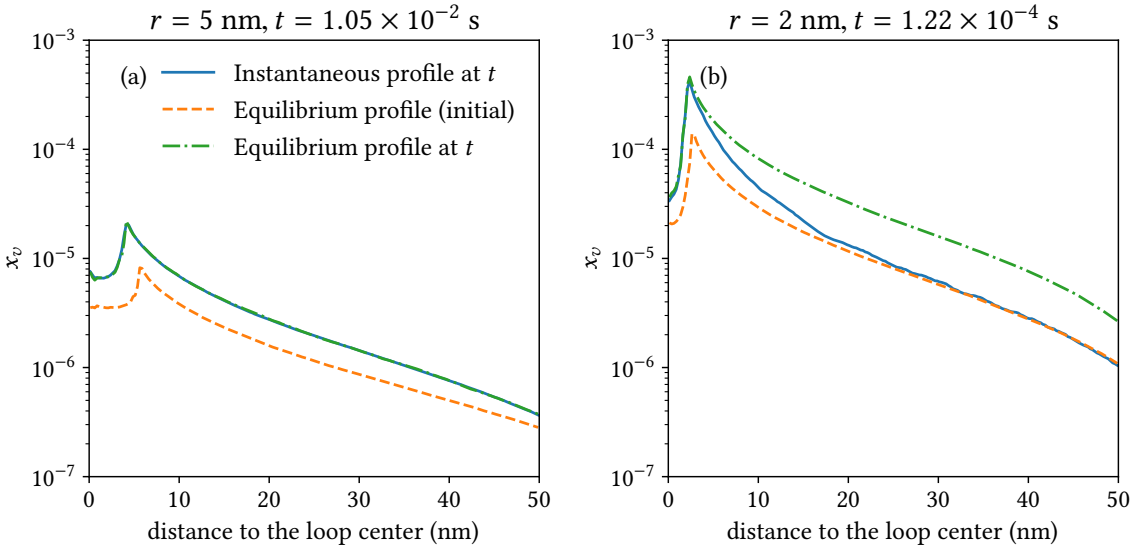

Figure 7. Vacancy atomic fraction profile as a function of the distance to the loop center, for two different loop radii ($r = 5$ nm and $r = 2$ nm), at times $t = 1.05 \times 10^{-2}$ s and $t = 1.22 \times 10^{-4}$ s respectively, corresponding to iteration 15 in Figs. 6-a and 6-b. The initial equilibrium profile and the equilibrium profile at time t are also shown.

shows that the quasi-static approximation is not valid in this case: vacancies cannot be emitted and migrate sufficiently far to build up the equilibrium profile before the local concentration near the loop changes appreciably.

Conclusion

In this work a model for emission of point defects by point defect sinks, suitable for object kinetic Monte Carlo (OKMC) simulations, has been presented. Local equilibrium near sinks is ensured by construction, whatever the level of description of point defects. In particular, it remains valid even if the effect of local stress on point defect diffusion is accounted for. The derivation and implementation of the model have been detailed for dislocation segments, but it can be generalized to other types of sinks (surfaces, grain boundaries, cavities, loops, etc.). The shrinkage of a single loop in a system containing surfaces has been modeled. Results are in good agreement with analytical formulas from the literature. In addition, since the OKMC framework does not require that the point defect concentration field is at equilibrium, it has been possible to verify to which extent this assumption is valid.

References

[1] J. Silcox and M. J. Whelan. Direct observations of the annealing of prismatic dislocation loops and of climb of dislocations in quenched aluminium. *Philos. Mag. A*, 5:1, 1960.

[2] S. Moll, T. Jourdan, and H. Lefaix-Jeuland. Direct observation of interstitial dislocation loop coarsening in α-iron. *Phys. Rev. Lett.*, 111:015503, 2013.

[3] K. H. Westmacott and R. E. Smallman. The formation, stability and effect on yield stress of cavities in neutron-irradiated aluminium. *Mater. Sci. Eng.*, 5:325, 1970.

[4] H. O. K. Kirchner. Size distribution of dislocation loops. *Acta Metall.*, 21:85, 1973.

[5] B. Burton and M. V. Speight. The coarsening and annihilation kinetics of dislocation loops. *Philos. Mag. A*, 53:385, 1986.

[6] I. M. Lifshitz and V. V. Slyozov. The kinetics of precipitation from supersaturated solid solutions. *J. Phys. Chem. Solids*, 19:35, 1961.

[7] C. Wagner. Theorie der Alterung von Niederschlägen durch Umlösen. *Z. Elektrochem.*, 65:581, 1961.

[8] F. R. N. Nabarro. In London Physical Society, editor, *Report of a Conference on the Strength of Solids*, page 75, 1948.

[9] C. Herring. Diffusional viscosity of a polycrystalline solid. *J. Appl. Phys.*, 21:437, 1950.

[10] J. Harper and J. E. Dorn. Viscous creep of aluminum near its melting point. *Acta Metall.*, 5:654, 1957.

[11] J. Weertman. Dislocation climb theory of steady-state creep. *Trans. Amer. Soc. Metals*, 61:681, 1968.

[12] J. P. Balbuena, M. J. Caturla, and E. Martinez. *Kinetic Monte Carlo Algorithms for Nuclear Materials Applications*, pages 1–22. Springer International Publishing, 2018.

[13] C. Domain and C. S. Becquart. *Object Kinetic Monte Carlo (OKMC): A Coarse-Grained Approach to Radiation Damage*, pages 1–26. Springer International Publishing, 2019.

[14] A. B. Sivak, V. M. Chernov, V. A. Romanov, and P. A. Sivak. Kinetic monte-carlo simulation of self-point defect diffusion in dislocation elastic fields in bcc iron and vanadium. *J. Nucl. Mater.*, 417:1067, 2011.

[15] G. Subramanian, D. Perez, B. P. Uberuaga, C. N. Tomé, and A. F. Voter. Method to account for arbitrary strains in kinetic Monte Carlo simulations. *Phys. Rev. B*, 87:144107, 2013.

[16] A. Vattré, T. Jourdan, H. Ding, M.-C. Marinica, and M. J. Demkowicz. Non-random walk diffusion enhances the sink strength of semicoherent interfaces. *Nat. Commun.*, 7:10424, 2016.

[17] D. Carpentier, T. Jourdan, Y. Le Bouar, and M.-C. Marinica. Effect of saddle point anisotropy of point defects on their absorption by dislocations and cavities. *Acta Mater.*, 136:323, 2017.

[18] M. J. Caturla, N. Soneda, E. Alonso, B. D. Wirth, T. Diaz de la Rubia, and J. M. Perlado. Comparative study of radiation damage accumulation in Cu and Fe. *J. Nucl. Mater.*, 276:13, 2000.

[19] D. R. Mason, X. Yi, M. A. Kirk, and S. L. Dudarev. Elastic trapping of dislocation loops in cascades in ion-irradiated tungsten foils. *J. Phys.: Condens. Matter*, 26:375701, 2014.

[20] J. Dalla Torre, J.-L. Bocquet, N. V. Doan, E. Adam, and A. Barbu. JERK, an event-based Kinetic Monte Carlo model to predict microstructure evolution of materials under irradiation. *Philos. Mag.*, 85:549, 2005.

[21] T. Jourdan, J.-L. Bocquet, and F. Soisson. Modeling homogeneous precipitation with an event-based Monte Carlo method: application to the case of Fe-Cu. *Acta Mater.*, 58:3295, 2010.

[22] C. McElfresh, Y. Cui, S. Dudarev, G. Po, and J. Marian. Discrete stochastic model of point defect-dislocation interaction for simulating dislocation climb. *Int. J. Plast.*, 136:102848, 2021.

[23] J. Friedel and M. Yoshida. On dislocation jogs as sources and sinks of vacancies. *Philos. Mag. A*, 31:229, 1975.

[24] C. Domain, C. S. Becquart, and L. Malerba. Simulation of radiation damage in Fe alloys: an object kinetic Monte Carlo approach. *J. Nucl. Mater.*, 335:121, 2004.

[25] Daniel T. Gillespie. A general method for numerically simulating the stochastic time evolution of coupled chemical reactions. *J. Comput. Phys.*, 22:403, 1976.

[26] A. B. Bortz, M. H. Kalos, and J. L. Lebowitz. A New Algorithm for Monte-Carlo Simulation of Ising Spin Systems. *J. Comput. Phys.*, 17:10, 1975.

[27] R. Siems. Mechanical interactions of point defects. *Phys. Stat. Sol.*, 30:645, 1968.

[28] T. Jourdan and A. Vattré. A continuous model including elastodiffusion for sink strength calculation of interfaces. *Comput. Mater. Sci.*, 153:473, 2018.

[29] J. P. Hirth and J. Lothe. *Theory of dislocations*. McGraw-Hill, 1968.

[30] R. W. Balluffi. Mechanisms of dislocation climb. *Phys. Stat. Sol.*, 31:443, 1969.

[31] A. Abu-Odeh, M. Cottura, and M. Asta. Insights into dislocation climb efficiency in FCC metals from atomistic simulations. *Acta Mater.*, 193:172, 2020.

[32] D. N. Seidman and R. W. Balluffi. Dislocations as sources and sinks for point defects in metals. In R. R. Hasiguti, editor, *Lattice Defects and Their Interactions*, page 913. Gordon and Breach Science Publishers, 1967.

[33] P. Ehrhart, P. Jung, H. Schultz, and H. Ullmaier. *Landolt–Börnstein, Numerical Data and Functional Relationships in Science and Technology*. Atomic Defects In Metals. Springer, 1991.

[34] H. Flyvbjerg and H. G. Petersen. Error estimates on averages of correlated data. *J. Chem. Phys.*, 91:461, 1989.

[35] P. S. Dobson, P. J. Goodhew, and R. E. Smallman. Climb kinetics of dislocation loops in aluminium. *Philos. Mag.*, 16:9, 1967.

[36] C. Bonafos, D. Mathiot, and A. Claverie. Ostwald ripening of end-of-range defects in silicon. *J. Appl. Phys.*, 83:3008, 1998.

[37] J. Ribis, F. Onimus, J.-L. Béchade, S. Doriot, A. Barbu, C. Cappelaere, and C. Lemaignan. Experimental study and numerical modeling of the irradiation damage recovery in zirconium alloys. *J. Nucl. Mater.*, 403:135, 2010.

[38] D. Mordehai, E. Clouet, M. Fivel, and M. Verdier. Introducing dislocation climb by bulk diffusion in discrete dislocation dynamics. *Philos. Mag.*, 88(6):899, 2008.

[39] B. Bakó, E. Clouet, L. M. Dupuy, and M. Blétry. Dislocation dynamics simulations with climb: kinetics of dislocation loop coarsening controlled by bulk diffusion. *Philos. Mag.*, 91:3173, 2011.

[40] Y. Gu, Y. Xiang, S. S. Quek, and D. J. Srolovitz. Three-dimensional formulation of dislocation climb. *J. Mech. Phys. Solids*, 83:319, 2015.

[41] I. Rovelli, S. L. Dudarev, and A. P. Sutton. Non-local model for diffusion-mediated dislocation climb and cavity growth. *J. Mech. Phys. Solids*, 103:121, 2017.

[42] D. N. Seidman and R. W. Balluffi. On the annealing of dislocation loops by climb. *Philos. Mag. A*, 13:649, 1966.

[43] A. Seeger and U. Gösele. Steady-state diffusion of point defects to dislocation loops. *Phys. Lett. A*, 61:423, 1977.

[44] W. Cai, A. Arsenlis, C. R. Weinberger, and V. V. Bulatov. A non-singular continuum theory of dislocations. *J. Mech. Phys. Solids*, 54:561, 2006.

[45] K. L. Baker and W. A. Curtin. Multiscale diffusion method for simulations of long-time defect evolution with application to dislocation climb. *J. Mech. Phys. Solids*, 92:297, 2016.

[46] C. H. Woo. The sink strength of a dislocation loop in the effective medium approximation. *J. Nucl. Mater.*, 98:279, 1981.

[47] T. Jourdan. Influence of dislocation and dislocation loop biases on microstructures simulated by rate equation cluster dynamics. *J. Nucl. Mater.*, 467:286, 2015.

[48] T. Jourdan. Simulation of macroscopic systems with non-vanishing elastic dipole components. *J. Mech. Phys. Solids*, 125:762, 2019.